

Heterostrain rules the flat-bands in magic-angle twisted graphene layers

Florie Mesple,^{1,*} Ahmed Missaoui,² Tommaso Cea,^{3,4} Loic Huder,⁵ Francesco Guinea,^{3,6} Guy Trambly de Laissardière,⁷ Claude Chapelier,¹ and Vincent T. Renard^{1,*}

¹*Univ. Grenoble Alpes, CEA, IRIG, PHELIQS, F-38000 Grenoble, France*

²*Laboratoire de Physique Théorique et Modélisation (UMR 8089),
CY Cergy Paris Université, CNRS, 95302 Cergy-Pontoise, France*

³*Imdea Nanoscience, Faraday 9, 28015 Madrid, Spain*

⁴*Instituto de Ciencia de Materiales de Madrid, CSIC,
Sor Juana Inés de la Cruz 3, Cantoblanco, 28049 Madrid, Spain*

⁵*European Synchrotron Radiation Facility (ESRF),
71 Avenue des Martyrs, 38000 Grenoble, France.*

⁶*Donostia International Physics Center, Paseo Manuel de Lardizábal 4, 20018 San Sebastián, Spain*

⁷*Laboratoire de Physique Théorique et Modélisation,
Université de Cergy-Pontoise-CNRS, F-95302 Cergy-Pontoise, France*

(Dated: December 7, 2020)

The moiré of twisted graphene bilayers can generate flat bands in which charge carriers do not possess enough kinetic energy to escape Coulomb interactions with each other^{1,2} leading to the formation of novel strongly correlated electronic states^{3,4}. This exceptionally rich physics relies on the precise arrangement between the layers.^{5,6} We survey published Scanning Tunnelling Microscope (STM) measurements^{7–16} to prove that near the magic angle, native heterostrain, the relative deformations between the layers, dominates twist in determining the flat bands. This is demonstrated at large doping where electronic correlations have a weak effect and where we also show that tip-induced strain can have a strong influence. In the opposite situation of low doping, we find that electronic correlation further normalizes the flat bands in a way that strongly depends on experimental details.

The strongly correlated electron physics recently observed in twisted graphene layers^{3,4} develops in flat bands^{1,2} which are very sensitive to the relative arrangement between the layers. For instance, the superconducting phase has been reported to occur in a very narrow range of rotation angle between the layers around the magic angle. As another illustration, hydrostatic pressure changes the interlayer distance which also strongly influences superconductivity^{5,6}. Heterostrain, the in-plane deformation of one layer with respect to the other is an ubiquitous source of modification of the relative arrangement between the layers^{7–16}. Experiments⁷ and theory^{17,18} have shown that heterostrain affects the flat bands which could have an impact on the strongly correlated electron physics. Bi, Yuan and Fu have even predicted that near the magic angle, the bandwidth becomes *insensitive* to the twist angle and that the effect of heterostrain is *dominant*,¹⁸ calling for systematic experimental study of its effect. Such program is however difficult to implement owing to the lack of controllability of heterostrain, and its inhomogeneity previously referred to as "twist angle disorder" and which was also found

to impact strongly correlated states at the macroscopic scale^{14,19}. In order to overcome these issues, we survey already published experimental STM data^{7–15} in view of quantifying the effect of homogeneous heterostrain on the physics of magic-angle twisted graphene layers.

Figure 1 presents typical STM images collected from Refs. 7–9. An immediate observation is that the STM images all look very similar. This is not surprising because these samples have a twist angle very close to one another. This similarity is only apparent as evidenced by the variety of shapes of the local density of states (LDOS) measured from the $dI/dV(V)$ spectroscopy (Fig. 1d). Despite the flat-bands should merge at the magic angle, the spectra of Ref. 8 and 9 show two van Hove singularities indicating that the flat bands are still separated. Their spacing ΔE_{exp} is doping dependent which has been attributed to electron-electron interactions.^{8–13} It can reach several tens of meV, even at large doping where correlations are not expected to renormalize strongly the bands. Still, while the two samples have a twist angle differing by only 0.1° , doping does not explain why their ΔE_{exp} differ by a factor 2-3. Sample to sample variation is obvious from other published data.^{10–15} Strikingly the data of Ref. 7 show a third peak at zero energy, a result which was recently reproduced¹⁶. In order to determine whether this variety in sample behaviour can be understood within the framework of heterostrain, we use the method described in Ref. 20 to determine the precise arrangement of the layers and calculate the corresponding local density of states using a tight-binding method.^{1,21,22}

Figure. 1a, b and c include our estimates of heterostrain. In all cases, biaxial heterostrain is smaller than uniaxial heterostrain which varies by a factor 3 from the smallest to the largest. Figure. 1d shows that the calculated local density of states agrees very well with experimental data. In particular the number of peaks is controlled by heterostrain which also influences their spacing pointing to a strong contribution of heterostrain to the observed phenomenology. The tight-binding calculations presented in Fig. 1f show that the van Hove singularities separate linearly with uniaxial heterostrain for all angle

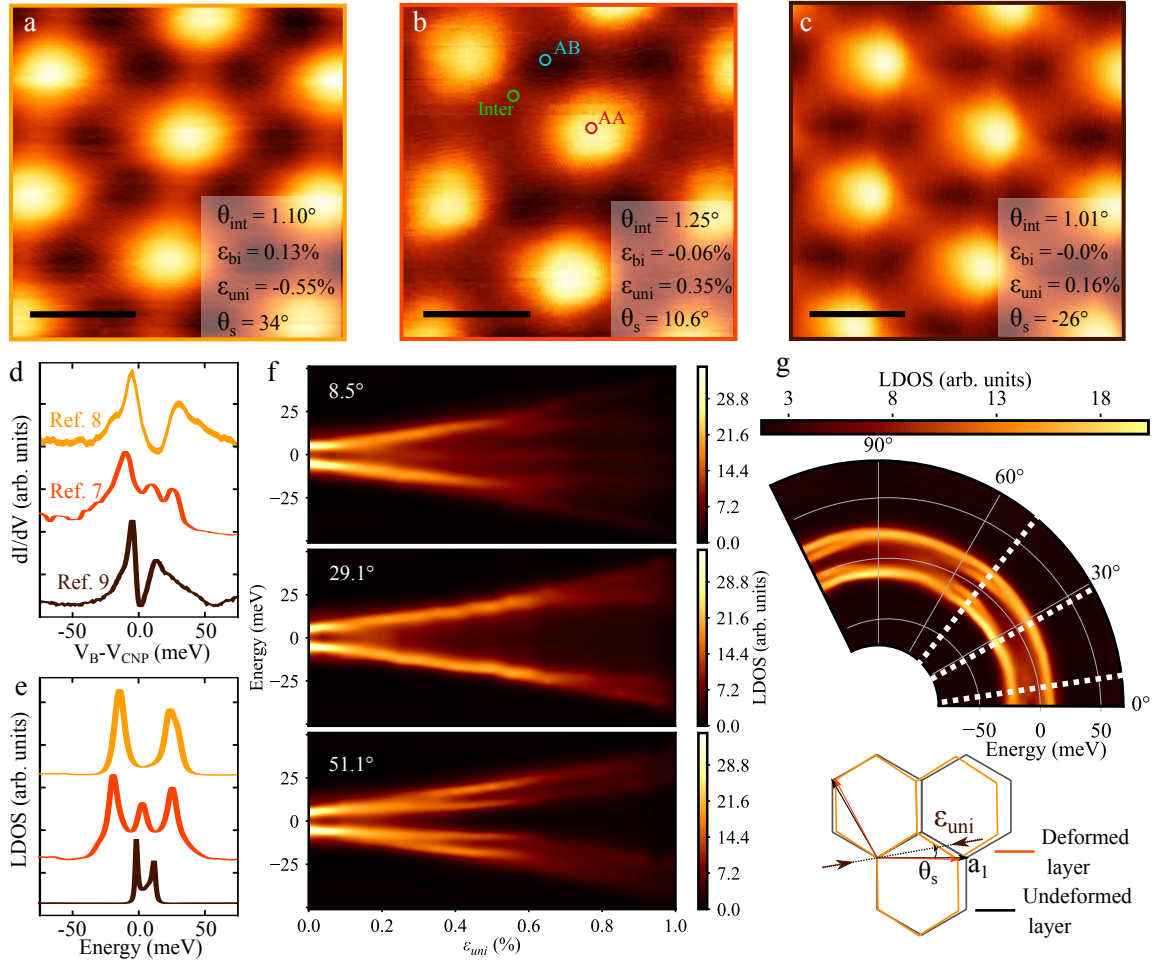


FIG. 1: Heterostrained twisted graphene layers. Panels **a**, **b** and **c** present STM images of twisted graphene layers near the magic angle adapted from Refs^{8,7} and⁹ respectively. The scale bar is 10 nm in each image. Insets present the parameters describing the relative arrangement of the layers in good agreement with estimates of the original studies.⁷⁻⁹ **d** Local density of states measured in the AA regions for each samples of panels **a**, **b** and **c**. **e** Corresponding tight-binding calculation of the LDOS including heterostrain. **f** Tight-binding prediction for the local density of states in AA regions as function of energy and for increasing uniaxial heterostrain. The variations are plotted for three different angles θ_s of application of heterostrain. **g** Local density of states calculated for 0.4 % of heterostrain applying along varying θ_s . The white dotted lines indicate the values of angles used in panel **f**. **h** Sketch of uniaxial heterostrain configuration. One layer is deformed by a uniaxial heterostrain applied along the direction defined by θ_s and then rotated by an angle θ with respect to the undeformed layer.

θ_s of application of heterostrain. This angle controls the splitting of the van Hove singularities (Fig. 1g) leading to three typical behaviours reported in Fig. 1f (See supplementary information and videos for more theoretical results). These results agree with those of the continuum model¹⁸. The more quantitative comparison of Fig. 2a shows that ΔE_{exp} converges to the value ΔE_{TB} predicted by our tight-binding calculation at large doping. This has to be expected because the effect of electronic correlations reduces with doping and the system evolves towards the non-interacting situation modeled by our tight binding calculations. It establishes that heterostrain controls the physics of twisted graphene layers near the magic angle at large doping. This can be viewed explicitly in Fig. 2b which shows that ΔE_{exp}^0 , the experimental spacings of

van Hove singularities at large doping, depends linearly on heterostrain as predicted by tight binding and the continuum model. On the contrary, the same data plotted as function of the twist angle do not show particular correlation with this parameter (Supplementary Fig. S5).

Figure 2c provides a deeper level of comparison between theory and experiment. It presents the relative difference between the ΔE_{TB} and the experimental ΔE_{exp}^0 as function of the tunnelling resistance $R_t = V_b/i_t$ (V_b and i_t are the tunnelling bias and current). The excellent agreement obtained for $R_t > 2 \text{ G}\Omega$ degrades below this value pointing to a possible influence of tip-induced strain which is known to be controlled by R_t .²³ The deformations seen in Fig 3a, b and c showing the evolution of the image of Fig. 1b for decreasing R_t corroborate this interpretation (The reader may also refer to Fig. S3 of

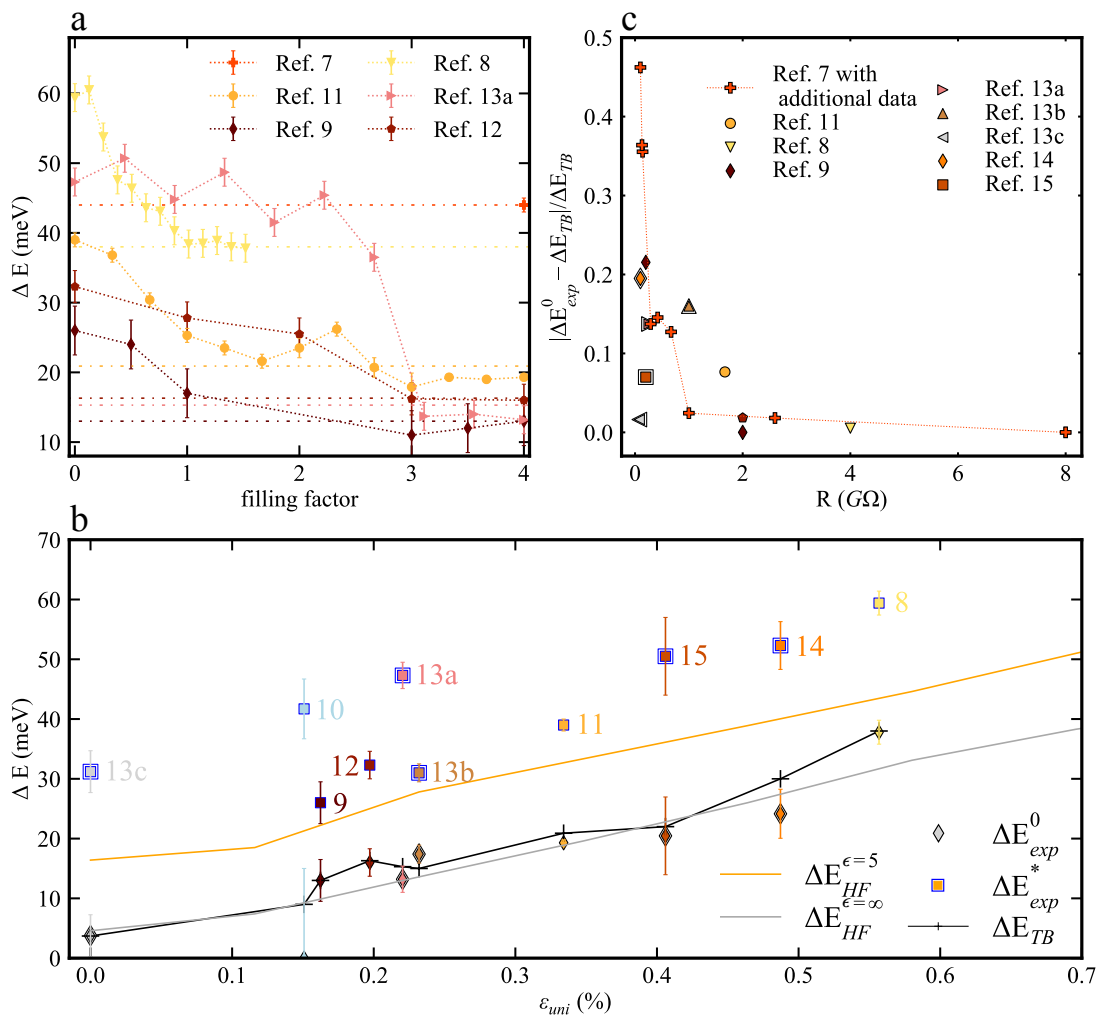


FIG. 2: Comparison between theory and experiments. **a** Representative doping dependence of the spacing between van Hove singularities. The horizontal line corresponds to prediction by tight-binding calculations with heterostrain. **b** Experimental spacing of van Hove singularities at large doping (ΔE_{exp}^0), zero doping (ΔE_{exp}^*), theoretical tight-binding (ΔE_{TB}), low-interaction Hartree-Fock ($\Delta E_{HF}^{\epsilon=\infty}$) and large interaction $\Delta E_{HF}^{\epsilon=5}$. Such presentation of all the data on a single graph is justified by i) the weak dependence of ΔE_{exp} on the twist angle near the magic angle (See Ref.¹⁸ and supplementary Fig. S5) and ii) the weak dependence of ΔE on θ_s if it is estimated as the spacing between the outermost singularities (Fig. 1g). This is also why the Hartree-Fock model was calculated for a twist angle of 1.1° and $\theta_s = 30^\circ$. On the contrary, ΔE_{TB} were calculated with the full relative arrangement of each experimental data and show a better agreement with experiments. The twist angle has still a small influence which explains the small deviations from a purely linear strain dependence. The measurements showing a cascade of transitions are indicated by a double border. **c** Relative deviation of ΔE_{exp}^0 to ΔE_{TB} as a function of the tunnelling resistance $R_t = V_b/i_t$. The figure includes new data for the sample of Fig. 1b.

Ref.⁹ for another example).

Figure 3 shows that while spatial variations of the LDOS at high R_t only reflect electronic localisation in AA regions, the response to tip-induced strain at low R_t strongly depends on the position on the moiré pattern. While AB regions are weakly affected (Fig. 3e), ΔE_{exp} is reduced by 40% at low tunnel resistance in AA regions indicating a flattening of the bands (Fig. 3d). The flattening culminates in intermediate regions between two AA regions where a 15 meV wide single LDOS peak signals that very flat bands can be engineered there (Fig. 3f). It is not surprising that these regions are the most sen-

sitive to tip-induced strain because they are characterized by an excess of elastic energy^{24–27} and are therefore more easily perturbed. We note that the tip may induce a complex strain pattern including hetero-, homostain as well as vertical displacement all of which depend on the position on the moiré. It follows that the relative arrangement between the layers can no longer be determined from STM images at low R_t and that the response to tip-induced strain is largely sample dependent. This is illustrated by Fig. S5 of Ref. 9 in which, contrary to our experiment, the spacing between van Hove singularities increases with decreasing R_t . We conclude that great

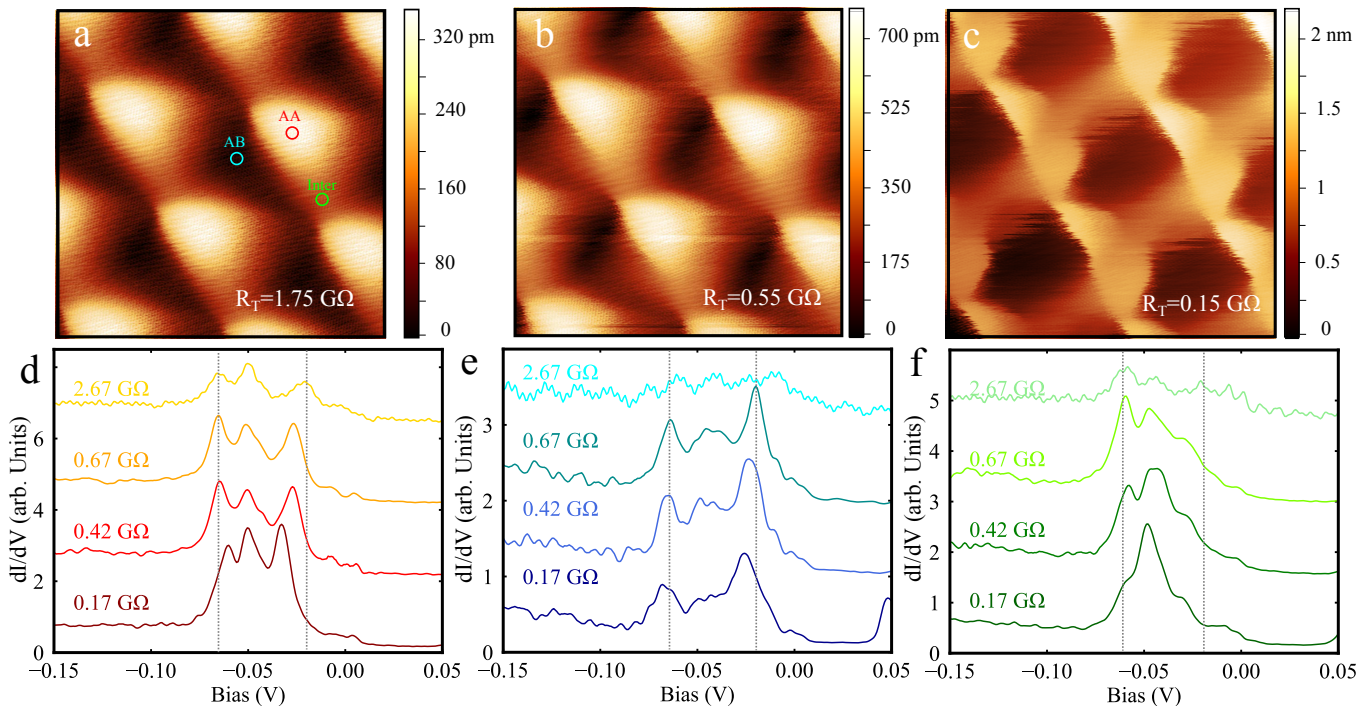


FIG. 3: Tip-induced strain. **a, b, c** STM images measured at decreasing tunneling resistance. The tunnelling set point is $i_t = 100$ pA and the bias is $V_b = 175$ mV in **a**, $V_b = 55$ mV in **b** and $V_b = 15$ mV in **c**. The images are 25×25 nm². **d, e, f** Local density of states measured by STM for decreasing tunnelling conductance in AA (**d**), AB (**e**) and intermediate regions (**f**). The vertical dotted lines are guides for the eyes to track the position of the LDOS peaks.

care is needed when discussing quantitatively experimental results and that the STM tip can be used to locally engineer the relative arrangement between the layers.

The very good agreement between experiments and theory obtained so far raises the question about the influence of heterostrain on electronic correlations which express most at zero doping.^{8–13} Figure 2b shows that ΔE_{exp}^* , the experimental spacing of van Hove singularities in this regime is increased by electronic correlations and tends to increase with strain. This tendency is well pictured by our Hartree-Fock calculations presented in Fig. 2b including both heterostrain and electronic correlations for the dielectric constant $\epsilon = 5$ (See Ref. 28 and supplementary information for the details). These calculations however underestimate ΔE_{exp}^* . Further increasing the effect of interactions by decreasing the dielectric constant does not lead to a better agreement especially at large strains where the low energy bands become so wide that they merge into the continuum of the higher energy bands and van Hove singularities can no longer be clearly defined (Supplementary information). Also the calculations do not capture the large experimental scatter of ΔE_{exp}^* which we were not able to correlate to any

experimental parameter (twist angle, heterostrain value or angle of application, bandwidths as measured by the FWHM of van Hove singularities, tunnelling resistance, temperature). The scatter also does not correlate with the appearance of polarized states leading to the cascade of transitions seen in some samples at intermediate fillings.^{13–15} This points to a strong sensitivity of electronic correlations to some additional experimental parameters beyond those investigated here. This could be due to the substrate or more generally to the detailed electrostatic environment as suggested by several studies reviewed in Ref. 29, and to atomic lattice relaxation effects²⁶ calling for a systematic experimental study of the effect of those parameters.

Returning to heterostrain, its strong impact on the flat bands of magic angle twisted graphene layers also calls for a systematic investigation of its influence on the strongly correlated phases and that of other moiré materials. In this context, it would be extremely desirable to be able to tune it. Alternatively, one could also rely of the variability in the fabrication process to generate a representative set of samples such as the one we have studied here.

* Electronic address: email: florie.mesple@cea.fr; vincent.renard@cea.fr

¹ Trambly de Laissardière, G., Mayou, D. & Magaud, L. Localization of Dirac Electrons in Rotated Graphene Bilayers.

- Nano Lett.* **10**, 804–808 (2010).
- ² Bistritzer, R. & MacDonald, A. H. Moiré bands in twisted double-layer graphene. *PNAS* **108**, 12233–12237 (2011).
 - ³ Cao, Y. et al. Magic-angle graphene superlattices: a new platform for unconventional superconductivity. *Nature* **55**, 43–50 (2019).
 - ⁴ Cao, Y. et al. Correlated insulator behaviour at half-filling in magic-angle graphene superlattices. *Nature* **556**, 80 (2019).
 - ⁵ Carr, S., Fang, S., Jarillo-Herrero, P. & Kaxiras, E. Pressure dependence of the magic twist angle in graphene superlattices. *Phys. Rev. B* **98**, 085144 (2018). URL <https://link.aps.org/doi/10.1103/PhysRevB.98.085144>.
 - ⁶ Yankowitz, M., Chen, S. & Dean, C. R. Tuning superconductivity in twisted bilayer graphene. *Science* **363**, 1059–1064 (2019).
 - ⁷ Huder, L. et al. Electronic spectrum of twisted graphene layers under heterostrain. *Physical Review Letters* **120**, 156405 (2018).
 - ⁸ Kerelsky, A. et al. Maximized electron interactions at the magic angle in twisted bilayer graphene. *Nature* **572**, 95–100 (2019).
 - ⁹ Choi, Y. et al. Electronic correlations in twisted bilayer graphene near the magic angle. *Nature Physics* **15**, 1174–1180 (2019).
 - ¹⁰ Jiang, Y. et al. Charge order and broken rotational symmetry in magic-angle twisted bilayer graphene. *Nature* **573**, 91–95 (2019).
 - ¹¹ Xie, Y. et al. Spectroscopic signatures of many-body correlations in magic-angle twisted bilayer graphene. *Nature* **572**, 101–105 (2019).
 - ¹² Zhang, Z., Myers, R., Watanabe, K., Taniguchi, T. & LeRoy, B. J. Probing the wave functions of correlated states in magic angle graphene. *Phys. Rev. Research* **2**, 033181 (2020). URL <https://link.aps.org/doi/10.1103/PhysRevResearch.2.033181>.
 - ¹³ Wong, D. & et al. Cascade of electronic transitions in magic-angle twisted bilayer graphene. *Nature* **582**, 198 (2020).
 - ¹⁴ Choi, Y. et al. Tracing out Correlated Chern Insulators in Magic Angle Twisted Bilayer Graphene. *arXiv* 2008.11746 (2020).
 - ¹⁵ Nuckolls, K. P. et al. Strongly Correlated Chern Insulators in Magic-Angle Twisted Bilayer Graphene. *arXiv* 2007.03810 (2020).
 - ¹⁶ Zhang, Y. et al. Electron interactions in strain-induced zero-energy flat band in twisted bilayer graphene near the magic angle. *arXiv* 2002.10073 (2020).
 - ¹⁷ Cosma, D. A., Wallbank, J. R., Cheianov, V. & Fal, V. I. Moiré pattern as a magnifying glass for strain and dislocations in van der Waals heterostructures. *Faraday Discussions* **173**, 137–143 (2014). URL <http://dx.doi.org/10.1039/C4FD00146J>.
 - ¹⁸ Bi, Z., Yuan, N. F. Q. & Fu, L. Designing flat bands by strain. *Phys. Rev. B* **100**, 035448 (2019). URL <https://link.aps.org/doi/10.1103/PhysRevB.100.035448>.
 - ¹⁹ Lu, X. & et al. Superconductors, orbital magnets and correlated states in magic-angle bilayer graphene. *Nature* **574**, 653–657 (2019).
 - ²⁰ Artaud, A. et al. Universal classification of twisted, strained and sheared graphene moiré superlattices. *Scientific Reports* **6**, 25670 (2016).
 - ²¹ Brihuega, I. et al. Unraveling the Intrinsic and Robust Nature of van Hove Singularities in Twisted Bilayer Graphene by Scanning Tunneling Microscopy and Theoretical Analysis. *Phys. Rev. Lett.* **109**, 196802 (2012).
 - ²² Trambly de Laissardière, G., Mayou, D. & Magaud, L. Numerical studies of confined states in rotated bilayers of graphene. *Phys. Rev. B* **86**, 125413 (2012).
 - ²³ Mamin, H. J., Ganz, E., Abraham, D. W., Thomson, R. E. & Clarke, J. Contamination-mediated deformation of graphite by the scanning tunneling microscope. *Phys. Rev. B* **34**, 9015–9018 (1986).
 - ²⁴ Alden, J. S. et al. Strain solitons and topological defects in bilayer graphene. *Proceedings of the National Academy of Sciences* **110**, 11256–11260 (2013). URL <https://www.pnas.org/content/110/28/11256>.
 - ²⁵ van Wijk, M. M., Schuring, A., Katsnelson, M. I. & Fasolino, A. Relaxation of moiré patterns for slightly misaligned identical lattices: graphene on graphite. *2D Materials* **2**, 034010 (2015). URL <https://doi.org/10.1088/2F2053-1583/2F2%2F3%2F034010>.
 - ²⁶ You, H. & et al. Atomic and electronic reconstruction at the van der Waals interface in twisted bilayer graphene. *Nature Materials* **18**, 448 (2019).
 - ²⁷ Gornostyrev, Y. N. & Katsnelson, M. I. Origin of the vortex displacement field in twisted bilayer graphene. *arXiv* 2006.11551 (2020).
 - ²⁸ Cea, T., Walet, N. R. & Guinea, F. Electronic band structure and pinning of Fermi energy to Van Hove singularities in twisted bilayer graphene: A self-consistent approach. *Phys. Rev. B* **100**, 205113 (2019). URL <https://link.aps.org/doi/10.1103/PhysRevB.100.205113>.
 - ²⁹ Balents, L., Dean, C. R., Efetov, D. K. & Young, A. F. Superconductivity and strong correlations in moiré flat bands. *Nature Physics* **16**, 725–733 (2020). URL <http://www.nature.com/articles/s41567-020-0906-9>.
 - ³⁰ Stewart, G. R. Heavy-fermion systems. *Rev. Mod. Phys.* **56**, 755–787 (1984). URL <https://link.aps.org/doi/10.1103/RevModPhys.56.755>.
 - ³¹ Lee, P. A., Nagaosa, N. & Wen, X.-G. Doping a Mott insulator: Physics of high-temperature superconductivity. *Rev. Mod. Phys.* **78**, 17–85 (2006). URL <https://link.aps.org/doi/10.1103/RevModPhys.78.17>.
 - ³² Stewart, G. R. Superconductivity in iron compounds. *Rev. Mod. Phys.* **83**, 1589–1652 (2011). URL <https://link.aps.org/doi/10.1103/RevModPhys.83.1589>.
 - ³³ Guinea, F. & Walet, N. R. Electrostatic effects, band distortions, and superconductivity in twisted graphene bilayers. *Proceedings of the National Academy of Sciences* 10947 (2018).
 - ³⁴ Xie, M. & MacDonald, A. H. Nature of the Correlated Insulator States in Twisted Bilayer Graphene. *Phys. Rev. Lett.* **124**, 097601 (2020). URL <https://link.aps.org/doi/10.1103/PhysRevLett.124.097601>.
 - ³⁵ Goodwin, Z., Vitale, V., Liang, X., Mostofi, A. A. & Lischner, J. Hartree theory calculations of quasiparticle properties in twisted bilayer graphene. *arXiv*:2004.14784 (2020).
 - ³⁶ Calderón, M. J. & Bascones, E. Interactions in the 8-orbital model for twisted bilayer graphene. *arXiv*:2007.16051 (2020).

Methods

Data collection

When possible, the raw data used in the survey were retrieved from the authors of the publications. Otherwise, the data were digitized from the corresponding publications. We could use the method of Ref.²⁰ to extract heterostrain for Refs.⁷⁻⁹ which had STM images with atomic resolution. The strength of this method is to isolate heterostrain from homostrain and possible artefacts due to the calibration of the piezoelectric tube. For Refs. (10, 11, 13a, 14, 15), we used the method described in Ref.⁸ to determine heterostrain. Although it does not allow to determine biaxial heterostrain we found it to provide good estimates of uniaxial heterostrain for the data of Refs.⁷⁻⁹. For Refs. (12, 13b, 13c), we did not have the data to do our own analysis and used the values of heterostrain provided by the authors. Error bars in Fig. 2 of main text present the uncertainty as estimated the full width at half maximum of a van Hove singularity.

STM measurements

We performed the measurements presented in Figure 3 of the main text in order to document the effect of tip-induced strain on the twisted graphene layers described in Ref.⁷. Tip-induced strain was changed by changing the bias for a given tunnel current in imaging conditions. In spectroscopic mode, the tip-sample interaction was defined by the set point prior to switching off the feedback loop and subsequent sweeping of the bias voltage between -200 mV and 200 mV. The $dI/dV(V)$ signal was measured using phase sensitive detection with a 2 mV oscillation at 263 Hz added to the tunnel bias. The dI/dV curves were normalised to 1 at -200 mV.

Acknowledgements

The authors thank E. Andrei, S. Nadj-Perge, for sharing their data and for interesting discussions. AM is supported by Paris//Seine excellence initiative (Grant No. 2019-055-C01-A0). FG and TC acknowledge funding from the European Commission, under the Graphene Flagship, Core 3, grant number 881603, and from grants NMAT2D (Comunidad de Madrid, Spain), SprQuMat and SEV-2016-0686, (Ministerio de Ciencia e Innovación, Spain)

Author contributions:

VTR,FM and CC defined the project. FM performed the data analysis from the literature and provided the cells for tight binding calculations which were performed

by AM and GTL. TC and FG performed Hartree-Fock calculations. LH, VTR and CC performed the STM experiments. VTR and FM wrote the manuscript with input from all the authors. VTR supervised the project.

Supplementary materials

Supplementary file and videos available on request to vincent.renard@cea.fr.